Bioorganic Chemistry 128 (2022) 106101

Contents lists available at ScienceDirect

Bioorganic Chemistry

journal homepage: www.elsevier.com/locate/bioorg

Synthesis and evaluation of benzoylbenzofurans and isoflavone derivatives as sirtuin 1 inhibitors with antiproliferative effects on cancer cells

Mamoalosi A. Selepe [a,*], Phaladi Kunyane [a], Pule Seboletswe [b], Shankari Nair [c], Nosipho Cele [b], Monique Engelbrecht [c], Daniël F. Joubert [d], Charlot Vandevoorde [c], Parvesh Singh [b,*], Molahlehi S. Sonopo [e,*]

[a] Department of Chemistry, University of Pretoria, Lynnwood Rd, Hatfield, Pretoria 0002, South Africa
[b] School of Chemistry and Physics, University of KwaZulu-Natal, P/Bag X54001, Westville, Durban 4000, South Africa
[c] Radiation Biophysics Division, Separated Sector Cyclotron Laboratory, NRF-iThemba LABS, Cape Town 7131, South Africa
[d] Department of Physiology, University of Pretoria, Lynnwood Rd, Hatfield, Pretoria 0002, South Africa
[e] Radiochemistry, South African Nuclear Energy Corporation Ltd, Pelindaba, Brits 0240, South Africa

ARTICLE INFO

Keywords:
Benzoylbenzofurans
Isoflavones
Sirtuin 1
MDA-MB-231

ABSTRACT

Isoflavone derivatives were prepared from benzoylbenzofuran precursors. The synthesized compounds were analyzed by 1D and 2D nuclear magnetic resonance (NMR) spectroscopy, as well as high-resolution mass spectrometry (HRMS) to confirm their structures. The benzoylbenzofuran and isoflavone analogues were evaluated for inhibition of sirtuin 1 (SIRT1) and cell proliferation in MDA-MB-231 triple-negative breast cancer (TNBC) cells. Several isoflavone and benzoylbenzofuran derivatives exhibited potent antiproliferative effects against the MDA-MB-231 cancer cell line. Most of the isoflavone derivatives attenuated SIRT1 activity to below 50%. The most active compounds were the isoflavone quinones **38**, **39**, and **40**, at IC_{50} values of 5.58 ± 0.373, 1.62 ± 0.0720, and 7.24 ± 0.823 μM, respectively. Importantly, the most active compound, 6-methoxy-4′,6′-dimethylisoflavone-2′,5′-quinone (**39**) displayed SIRT1 inhibitory activity comparable to that of the reference compound, suramin. The *in silico* docking simulations in the active site of SIRT1 further substantiated the experimental results and explored the binding orientations of potent compounds in the active site of the target.

1. Introduction

Sirtuins (SIRTs) are a group of nicotinamide adenine dinucleotide (NAD^+) dependent class III histone deacetylase (HDAC) enzymes [1,2]. Seven SIRTs (SIRT1-7) have been identified in mammals, with each protein sharing a conserved NAD^+ binding domain but with diverse enzymatic activity, that regulates multiple different metabolic pathways [1,2]. This diversity in function of SIRTs, and their implication in diseases such as cancer makes them ideal targets in drug discovery and development [1,2]. The most studied member of the sirtuin family is SIRT1. In breast cancer, SIRT1 can act as both a tumor suppressor and a tumor promoter [3]. This paradoxical function of SIRT1 is dependent on the breast cancer subtype [3]. Ryu's group reported that reduced expression of SIRT1 in luminal A breast cancer is predictive of lymph node metastasis [4], whereas increased expression of SIRT1 in TNBC is associated with an increase in tumor invasion and lymph node metastasis [5,6]. SIRT1 can act as a tumor promoter by inactivating p53 through deacetylation [2]. It has also been reported to promote tumor invasion and metastasis by modulating the epithelial-mesenchymal transition (EMT) process [6]. The modulation of EMT by SIRT1 has been shown to have an effect on breast cancer stem cells (BCSCs) through the SIRT1-mediated activation of the Wnt signaling pathway [7]. In several studies, SIRT1 inhibitors have been reported to exhibit both *in vitro* and *in vivo* anticancer activity [8,9,10], enhance the sensitivity of multidrug-resistant cells to chemotherapeutic agents, and inhibit proliferation of drug-resistant cancer cells [9,10,11]. Inhibition of SIRT1 has been shown to block the Wnt signaling cascade, decreasing the stemness of cancer stem cells (CSCs) and reducing EMT, which leads to a subsequent reduction in metastasis [7,12,13,14]. An approach that targets SIRT-mediated EMT and CSCs renewal through SIRT1 modulation, as an adjuvant to conventional chemotherapy, has been proposed as a potential strategy for overcoming multidrug resistance in breast

* Corresponding authors.
E-mail addresses: mamoalosi.selepe@up.ac.za (M.A. Selepe), Singhp4@ukzn.ac.za (P. Singh), Molahlehi.Sonopo@necsa.co.za (M.S. Sonopo).

https://doi.org/10.1016/j.bioorg.2022.106101
Received 20 June 2022; Received in revised form 1 August 2022; Accepted 12 August 2022
Available online 17 August 2022

cancer [7].

Over the years, natural products have shown potential as sources of new anticancer agents [15]. Natural product-based anticancer drugs depended mainly on microtubule-targeting compounds such as taxanes, vinca alkaloids, and epithilone derivatives [16]. Other natural compounds that have shown potential in cancer prevention and therapy are isoflavonoids [17]. The antitumor activity of isoflavonoids is mainly ascribed to their oestrogenic effects as well as their ability to modulate several signaling pathways that are involved in different stages of cancer development [17]. Consequently, several drugs developed based on the isoflavonoid nucleus have been under investigation. These include three generations of anticancer drugs derived from genistein framework such as phenoxodiol, Me-344, and Trilexium (TRX-E-009–1), respectively (Fig. 1) [18,19,20]. The antitumor activity of the compounds was enhanced exponentially from one generation to the other [20], as a result of the different mechanisms of action exhibited by each group [20,21]. The third generation of benzopyrans, Cantrixil (TRX-E-002-1) and TRX-E-009-1 were determined to be tubulin polymerization inhibitors *in vitro* and *in vivo*. Importantly, the third generation strongly inhibited ovarian CSCs [20,21]. The improved activity observed with each generation demonstrates the importance of the isoflavonoid scaffold for utilization in anticancer drug development. Recently, the FDA approved Umbralisib, a kinase inhibitor containing an isoflavonoid motif, for marginal zone lymphoma and follicular lymphoma [22].

In 2019, we reported a synthetic route of isoflavones from methoxybenzoylbenzofurans [23]. Benzoylbenzofurans also exhibit important biological activities and have been employed as lead compounds in the development of antitumor drugs [24,25,26]. Previous studies have shown that benzofuran derivatives exhibit inhibition of microtubules, oestrogen receptors, angiogenesis, and glycogen synthase kinase [27]. Therefore, the developed synthetic methodology enables switching from one scaffold of pharmaceutical importance (benzoylbenzofuran) to another (isoflavone), thereby rendering a library of benzoylbenzofuran and isoflavone derivatives for exploration of their biological activities. In this study, we further demonstrated the application of our synthetic method in the preparation of an analogue of the natural isoflavone hemerocallone [28] and evaluated the benzoylbenzofuran precursors and their isoflavone counterparts for inhibitory effects on SIRT1 enzyme and cancer cells. Additionally *in silico* docking simulations were also performed to gain further insights into the host–guest relationship of potent compounds with SIRT1.

2. Results and discussion

Synthesis of 2′,5′-dimethoxy-6,7-methylenedioxyisoflavone (**5**), an analogue of the natural isoflavone hemerocallone [28] commenced with Friedel-Crafts acylation of sesamol (**1**) to afford methylenedioxyacetophenone **2** in 61% yields (Scheme 1). Methylation of **2** and subsequent condensation of the acetophenone **3** with DMF-DMA, followed by 1,4-Michael addition with 1,4-benzoquinone in AcOH delivered the benzoylbenzofuran **4** in 44% yields. Treatment of the benzoylbenzofuran **4** with 98% TMSI in DMF and subsequent methylation of the resulting product with MeI afforded the targeted isoflavone **5**.

Reagents and conditions: a) Ac_2O, $BF_3.OEt_2$, 80 °C, 8 h, b) MeI, DMF, K_2CO_3, 100 °C, 4 h c) i: DMF-DMA, 100 °C, 12 h, ii: *p*-benzoquinone, AcOH, rt, 12 h d) i: DMF, TMSI, 85 °C, 36 h, ii: MeI, DMF, K_2CO_3, 100 °C, 3 h

Since the synthesis of isoflavones from benzoylbenzofurans is still a newly established protocol, it was necessary to assign the structures of the synthesized compounds unambiguously. Therefore, the intermediates and final products were analyzed using high-resolution mass spectrometry (HRMS) and one-dimensional and two-dimensional nuclear magnetic resonance (1D and 2D NMR) spectroscopy to confirm their structures. For instance, the ^{1}H NMR spectrum of **4** showed two one-proton singlets for the A-ring protons at δ_H 6.96 (H-3′) and 7.00 (H-6′), and an ABX spin system for the B-ring protons at δ_H [7.47 (d, J = 8.9 Hz, 1H, H-7); 6.83 (dd, J = 8.9, 2.5 Hz, 1H, H-6); 7.42 (d, J = 2.8 Hz, 1H, H-4). The signals for the methoxy, methylenedioxy, oxymethine and hydroxy groups were observed at δ_H 3.67 (s, 3H, OCH_3-2′); 6.08 (s, 2H, OCH_2O); 8.35 (s, 1H, H-2); and 9.46 (s, 1H, OH-5), respectively. The ^{13}C spectrum of compound **4** displayed 17 carbon signals that consisted of six aromatic hydrocarbons signals at δ_C 95.8 (CH, C-3′); 108.3 (CH, C-6′); 106.3 (CH, C-4), 114.2 (CH, C-6), 112.1 (CH, C-7), and 155.3 (CH, C-2); three non-hydrogenated tertiary carbon signals at δ_C 121.5 (C, C-1′), 121.9 (C, C-3), and 125.2 (C, C-3a); five oxygenated tertiary carbon signals at δ_C 140.7 (C, C-5′), 149.1 (C, C-7a), 150.2 (C, C-4′), 153.3 (C, C-2′), and 154.7 (C, C-5); and finally the signals of the methoxy, methylenedioxy and ketocarbonyl appeared at δ_C 56.5 (CH_3, OCH_3-2′), 101.8 (CH_2, OCH_2O), and 188.5 (C, C═O), respectively. The assignment of all carbon signals was facilitated by HSQC and HMBC data. The observed key HMBC correlations are shown in Fig. 2. The adjoined B and the C-rings of the benzofuran were established by HMBC correlations from H-2 (δ_H 8.35) to δ_C 149.1 (C-7a), 125.2 (C-3a) and 121.9 (C-3); and those of the hydroxy group (OH-5) to δ_C 154.7 (C-5), 114.2 (CH-6) and 106.3 (CH-4). The tertiary oxygenated carbon signals of the A-ring were

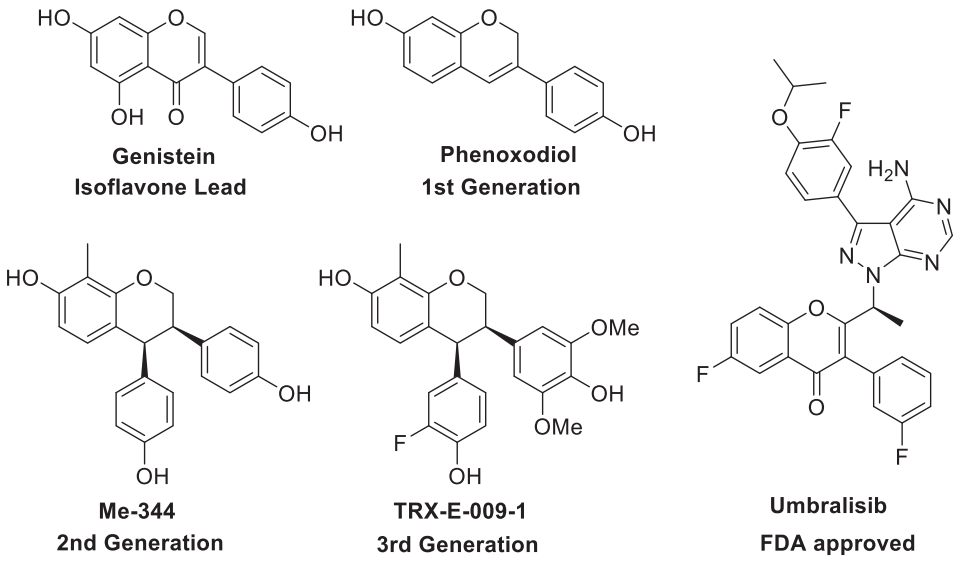

Fig. 1. Investigational antitumor derivatives based on genistein and approved isoflavone-bearing anticancer drug.

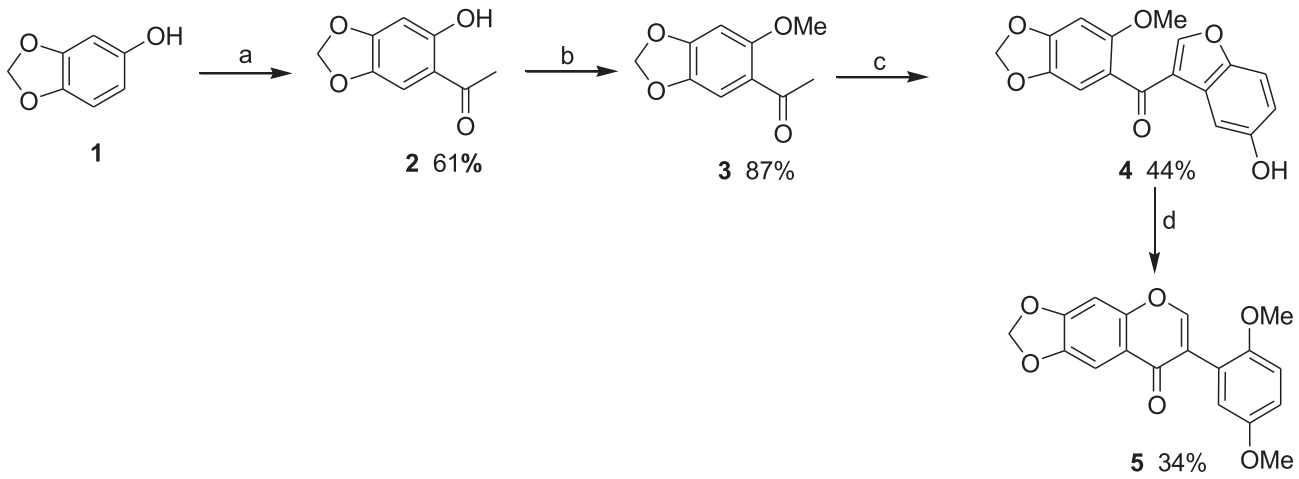

Scheme 1. Preparation of benzoylbenzofuran **4** and isoflavone **5.**

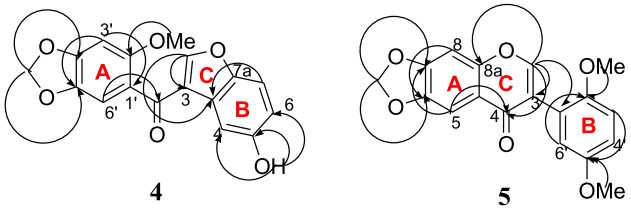

Fig. 2. Key HMBC correlations observed for compounds **4** and **5.**

assigned based on the HMBC correlation of the methoxy group to δ_C 153.3 (C-2′) and those of the methylenedioxy group to δ_C 150.2 (C-4′) and 140.7 (C-5′). The A-ring aromatic proton signals at δ_H 7.00 (H-6′) and 6.96 (H-3′) also showed long-range correlations to 188.5 (C═O), 121.5 (C-1′), 140.7 (C-5′) and 150.2 (C-4′). Finally, the molecular ion peak at *m/z* 313.0712 $[M + H]^+$ (calcd. for $C_{17}H_{13}O_6$ 313.0707) in its HRMS confirmed the assigned structure.

The molecular formula of the isoflavone **5** on the other hand was confirmed to be $C_{18}H_{14}O_6$ from the HRMS data [*m/z* 327.0876 $[M + H]^+$ (calcd. for $C_{18}H_{15}O_6$ 327.0863)]. The ^{1}H NMR spectrum of **5** displayed three one-proton singlets at δ_H 7.30 (H-8), 7.37 (H-5), 8.26 (H-2); and a two-protons singlet at δ_H 6.23 (OCH_2O), for the chromone core (A-and C-rings) and the methylenedioxy group substituent. The proton signals on the B-ring and that of the methoxy substituents were observed at δ_H 6.85 (d, $J = 3.1$ Hz, 1H, H-6′); 6.94 (dd, $J = 9.0$, 3.1 Hz, 1H, H-4′); 7.01 (d, $J = 9.0$ Hz, 1H, H-3′); δ 3.66 (s, 3H, OCH_3-2′); 3.72 (s, 3H, OCH_3-5′). The ^{13}C NMR spectrum of the isoflavone **5** displayed 18 carbon resonances. The signals for the two methoxy groups and one signal for methylenedioxy group appeared at δ_C 55.5 (OCH_3-5′), 56.1 (OCH_3-2′), and 102.9 (OCH_2O), respectively. Also present were five arene signals at δ_C 98.3 (CH, C-8), 101.3 (CH, C-5), 112.4 (CH, C-3′), 114.0 (CH, C-4′), and 117.5 (CH, C-6′), and that of oxygenated alkene at δ_C 154.2 (CH, C-2). Moreover, eight tertiary carbon resonances at δ_C 118.5 (C, C-4a), 121.4 (C, C-3); 121.9 (C, C-1′); 146.1 (C, C-6); 151.6 (C, C-2′); 152.6 (C, C-8a); 152.8 (C, C-7); 153.0 (C-5'); and a ketocarbonyl signal at δ_C 173.7 (C═O, C-4) were also present in the spectrum. The chromone core (A- and C-rings) was established based on key HMBC correlations from H-2 (δ_H 8.26) to δ_C 152.6 (C-8a), from the OCH_2O (δ_H 6.23) to δ_C 146.1 (C-6) and δ_C 152.8 (C-7), from H-5 (δ_H 7.37) to δ_C 173.7 (C═O, C-4), and from H-8 (δ_H 7.30) to δ_C 118.5 (C-4a). The B-ring signals were assigned based on key HMBC correlations that included correlations from H-2 (δ_H 8.26) to δ_C 121.9 (C-1′), from the methoxy signals (δ_H 3.66 and 3.72) to δ_C 151.6 (C-2′) and δ_C 153.0 (C-5′), from H-3′ (δ_H 7.01) to δ_C 153.0 (C-5′) and δ_C 121.9 (C-1′). This confirmed the successful reassembly of the benzoylbenzofuran **4** and subsequent methylation into the isoflavone **5.**

The SIRT1 inhibitory activity of benzoylbenzofurans and corresponding isoflavone analogues was evaluated using a fluorogenic peptide that was deacetylated in the presence of NAD^+. The representative compounds tested are shown in Fig. 3 and the results in Table S1 (Supplementary information) and Fig. 4. As shown in Table S1 and Fig. 4, most of the benzoylbenzofurans did not significantly attenuate the SIRT1 activity. Starting with the halogenated derivatives, the most active benzoylbenzofurans were those with 5′-halogen substituents (**6** and **9**) on the A-ring of the benzoylbenzofuran. The compounds **6** and **9** reduced SIRT1 activity to 42.2% and 45.9%, respectively at the test concentration of 100 μM. The 4′-halogenated derivatives **7** and **8** did not demonstrate pronounced effects. On the contrary, the isoflavone **28** that resulted from **7** suppressed SIRT1 activity to 7.31%. The benzoylbenzofurans **10**, **11**, and **12** with *p*-dimethoxy substituents and resorcinol moiety resulted in SIRT1 activity greater than 90%. Their isoflavone counterparts **29**, **30**, and **31** reduced the SIRT1 activity to 14.6%, 21.3%, and 49.9% respectively. The relatively higher inhibitory potential of compounds **29** and **30** compared to **31** highlights the importance of the 6-methoxy/hydroxy group on the SIRT1 inhibitory activity of the isoflavones. Evaluation of the benzoylbenzofurans with the increased number of substituents on the A-ring revealed one moderately active pyrogallol derivative **16**, with a free hydroxy group at the 2′ position. The isoflavone analogue **35** attenuated SIRT1 activity to 10.6%. The benzoylbenzofurans **13** and **14** with phloroglucinol scaffold showed activities above 80%, while the resulting isoflavones **32**, **33**, and **34** attenuated the SIRT1 activity to 3.59%, 21.5%, and 69.5%, respectively. The higher inhibitory activity observed for 5,7-dimethoxyisoflavone **32** and lower inhibitory activity observed for the demethylated phloroglucinol derivatives **33** and **34** suggest that the free hydroxy groups on the A-ring were unfavorable for the SIRT1 inhibitory activity of the isoflavones.

The effect of the substituents on the B-ring was also evaluated. The first two benzoylbenzofurans with methyl substituents on the B-ring (**17** and **18**) decreased the SIRT1 activity to 85.6% and 42.1%, respectively, while their corresponding isoflavone derivatives **36** and **37** suppressed the SIRT1 activity to 16.8% and 42.7%. The compounds **19**, **20**, **21**, and **22** with resorcinol moiety exhibited activities ranging from 96.0% to 65.5%. Those with *p*-dimethoxy groups on the A-ring (**23** and **24**) showed SIRT1 activity of 80.4% and 53.4%, respectively. Interestingly, the resulting isoflavone quinones **38** and **39** strongly attenuated SIRT1 activity to sub-zero values at the concentration of 100 μM. The last set of benzoylbenzofurans that were evaluated for their potential to modulate the SIRT1 activity were compounds **25** and **26**. The two compounds exhibited SIRT1 activity of 95.2% and 80.4%, respectively. On the other hand, their isoflavone counterpart, 7-methoxy-8-hydroxyisoflavone quinone **40** induced 2.6% SIRT1 activity.

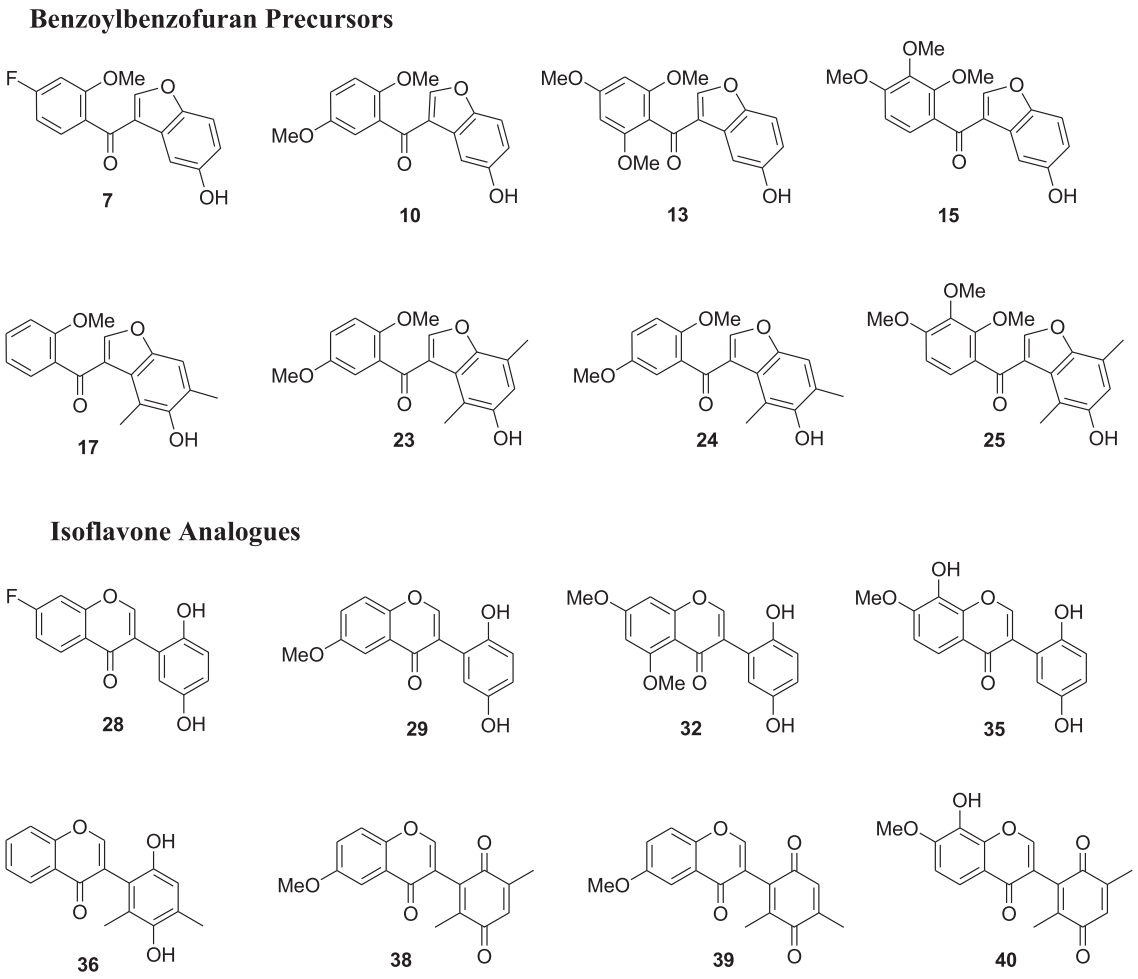

Fig. 3. Selected benzoylbenzofuran and isoflavone analogues.

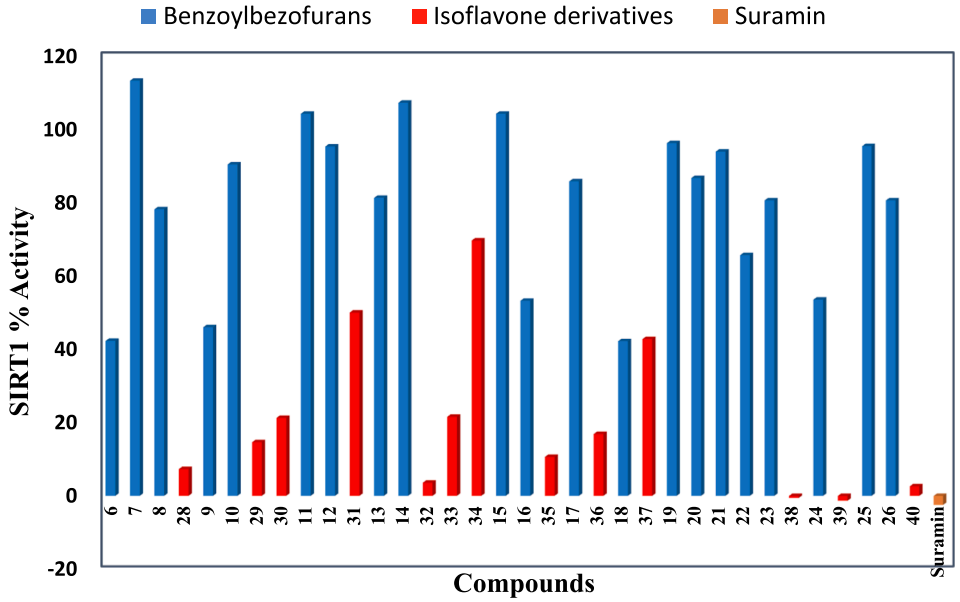

Fig. 4. SIRT1 activity upon treatment with 3-benzoylbenzofuran and isoflavone analogues.

The IC_{50} values of the isoflavone derivatives that strongly reduced the SIRT1 activity were determined as shown in Table 1. From these results is observed that the isoflavone analogue **39**, exhibited inhibitory effects with an IC_{50} of 1.62 μM, comparable to that of the reference compound suramin (IC_{50} = 1.75 μM).

We next evaluated the antiproliferative effects of the most promising

Table 1
IC_{50} values for the most potent SIRT1 inhibitors.[a]

Compound ID	SIRT1 Inhibition IC_{50} (μM)
28	17.8 ± 1.51
32	34.9 ± 2.66
38	5.58 ± 0.373
39	1.62 ± 0.0720
40	7.24 ± 0.823
Suramin	1.75

[a] Tests performed in triplicates.

SIRT1 inhibitors and some benzoylbenzofurans in a human TNBC cell line, MDA-MB-231, using the MTT (3-(4,5-dimethylthiazol-2-yl)-2,5-diphenyltetrazolium bromide) assay. The IC_{50} values of the target compounds and those of the standard drugs are collated in Table 2. The antiproliferative results revealed that both the benzoylbenzofuran and the isoflavonoid derivatives show activity in the MDA-MB-231 cells, inhibiting proliferation. The most active compounds were the newly synthesized benzoylbenzofuran **4** and the 5-bromobenzoylbenzofuran **27**, which showed antiproliferative activity with IC_{50} values of 3.86 and 5.68 μM, respectively. Contrarily, isoflavone **5** showed lower potency (IC_{50} = 9.53 μM) compared to its benzoylbenzofuran counterpart **4**. The most active SIRT1 inhibitors **38**, **39**, and **40** inhibited MDA-MB-231 cell growth at IC_{50} values of 6.39, 6.34, and 9.52 μM, respectively. From the results, it is observed that the activity of isoflavone derivatives was dependent on the nature of the substitution pattern on the A-ring of the isoflavonoid moiety. The isoflavone quinones **39** and **40** with the methoxy group at C-6 in the A-ring showed increased growth inhibition than all isoflavone derivatives evaluated.

The most active SIRT1 inhibitor **39** potently inhibited MDA-MB-231 cell growth (IC_{50} = 6.34 μM) than all other isoflavonoid derivatives tested in this study. However, its activity was lower than that of the two benzoylbenzofurans **4** and **27** (IC_{50} = 3.86 and 5.68 μM, respectively). Benzofurans are well known for their anticancer properties [25,27]. Therefore, it is not surprising that the two compounds were active on the cancer cells. Although compound **39** exhibited lower cell inhibitory activity than the benzofurans **4** and **7**, its activity is higher than that reported for the known SIRT1 inhibitor, suramin (IC_{50} = 7 μM) [29]. This, coupled with the pronounced SIRT1 inhibitory activity of **39** warrants further studies of this compound on breast cancer and other cancers for the development of more active derivatives.

The potency of promising compounds **28**, **32**, **38**, **39**, and **40** was further studied *in silico* using the reported crystal structure of SIRT1 (SIRT1; PDB ID: 4I5I). The calculations were computed with Schrödinger molecular modeling suite (release 2021-2) and induced-fit docking (IFD) protocol. The docking protocol, IFD, was selected as it combines both Glide docking and Prime refinement modules to predict ligand binding modes while allowing structural flexibility of the receptor to produce a reliable model of the ligand-receptor complex. Therefore, the identified compounds were docked at the active site of SIRT1 to further elucidate the observed antiproliferative effect against MDA-MB-231. The docking results generally showed a similar trend to the IC_{50} values of the examined compounds.

The biological data highlighted compound **39** as the most potent antiproliferative agent from the chromene-4-one series and this was further confirmed by the superior ligand-receptor affinity depicted by the binding free energy of −70.51 kcal.mol^{-1} and a docking score of −10.922 (Table 3). The higher docking score signified a perfect snuggling of the ligand in the active site while the high binding free energy showed a stable conformation of the complex. However, the latter is dependent on glide emodel and glide energy parameters. The results also indicate that the stable binding of compound **39** in the active site may also be assisted by the HOH717 water molecule. Compound **39** carbonyl from the quinone ring formed a water-mediated hydrogen bond with Gln345 and another hydrogen bond with Ala262. The adjacent carbonyl group of the ring also formed hydrogen bonds with Ser442 and Lys444. The chromene core carbonyl formed a hydrogen bond with Arg274 while the oxygen formed hydrogen bonds with His363. These rings also formed *pi-pi* stacking with Phe273 and His363, respectively (Fig. 5). The optimal activity of compound **39** as further expanded by its interaction in the active site is comparable to that of the reference compound suramin. Suramin complex produced a docking score and binding energy of −6.145 and −59.20 kcal.mol^{-1} respectively.

The 3-fold reduced potency of compound **38** was evidenced by the lower docking score (−8.904) and binding free energy (-65.04 kcal.mol^{-1}) of its SIRT1 complex. The carbonyl group of the quinone ring formed hydrogen bonds with Arg274 and Tyr280 residues. The chromene oxygen formed a hydrogen bond with His363 while the ring carbonyl unit interacted with the protonated amino group of Arg274. The SIRT1 complex also featured His363 *pi-pi* stacking with the chromene core ring while the electron-donating methoxy substituent formed hydrogen bonds with Ser441 and Ser442 (Fig. 5).

The SIRT1-**40** complex on the other hand gave a docking score of −7.470 and binding free energy of −58.23 kcal.mol^{-1}. The significant drop in glide emodel and glide energy validates the poor binding affinity compared to compound **38** and **39** complexes. A closer look at the SIRT1-**40** complex showed that the quinone carbonyl formed only two hydrogen bonds with the amino groups of Arg274 and interactions with the carbonyl group were absent. The hydroxy group of the chromene aromatic ring formed hydrogen bonds with Ala262 and Ser441 and a water-mediated hydrogen bond with Gln345 and Asn346. Also, these rings formed a *pi*-cation interaction with the protonated amino group of Arg274 while the methoxy group formed hydrogen bonds with Ser441, Ser442, Ala262, and Gly263 (Fig. 6).

From the SIRT1-**28** complex, the hydroxy group of the hydroquinone ring formed hydrogen bonds with Gln345 and Ser441 while one of the rings maintained the *pi*-cation interaction with the Arg274 protonated amino group. The chromene carbonyl formed hydrogen bonds with Ser442 and Arg274, even as the oxygen group formed a hydrogen bond with Gly263 (Fig. 6). Substituting a fluoro unit for the methoxy in this

Table 2
IC_{50} values (μM) from the MTT assay conducted in MDA-MB-231, human TNBC cells.

Compound ID	IC_{50} (μM)	CI of IC_{50} (μM)
4	3.86	2.97–5.01
20	6.45	4.55–9.15
23	7.93	6.06–10.4
24	9.95	9.23–10.7
27	5.68	5.20–6.21
5	9.53	8.34–10.9
38	6.39	4.42–9.23
39	6.34	5.13–7.84
40	9.52	7.50–12.1
Combretastatin A4	2.46	1.13–5.35
Doxorubicin	1.67	0.657–4.44

Table 3
Induced fit docking (IFD) and MM-GBSA (ΔG bind) calculations of selected compounds.

Ligand	IC_{50} (μM)	Docking score	Glide Emodel	Glide energy	ΔG bind (kcal.mol^{-1})
39	1.62 ± 0.0720	−10.922	−81.942	−57.363	−70.51
38	5.58 ± 0.373	−8.904	−86.890	−56.099	−65.04
40	7.24 ± 0.823	−7.470	−65.946	−49.935	−58.23
28	17.8 ± 1.51	−6.896	−65.981	−45.132	−56.26
32	34.9 ± 2.66	−6.083	−60.945	−45.588	−54.43
Suramin	1.75	−6.145	−124.572	−78.339	−59.20

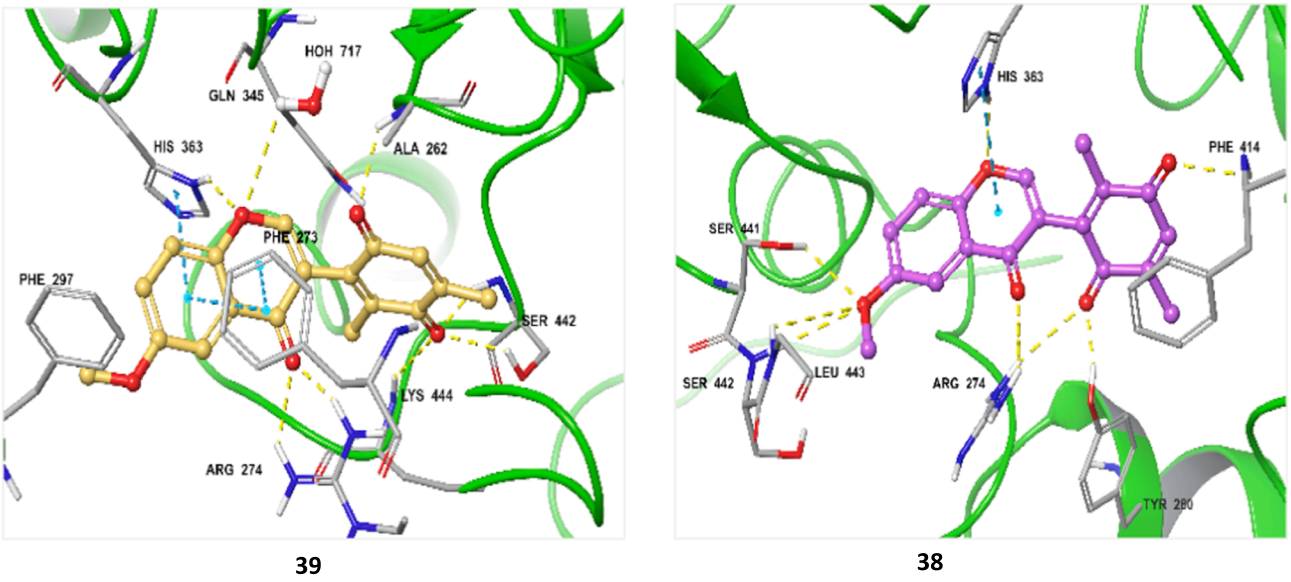

Fig. 5. Predicted binding modes of compounds **39** and **38** at the active site of SIRT1. Protein-ligand interactions are shown as dashed lines; hydrogen bond (yellow), pi-pi stacking (light-blue) pi-cation (green).

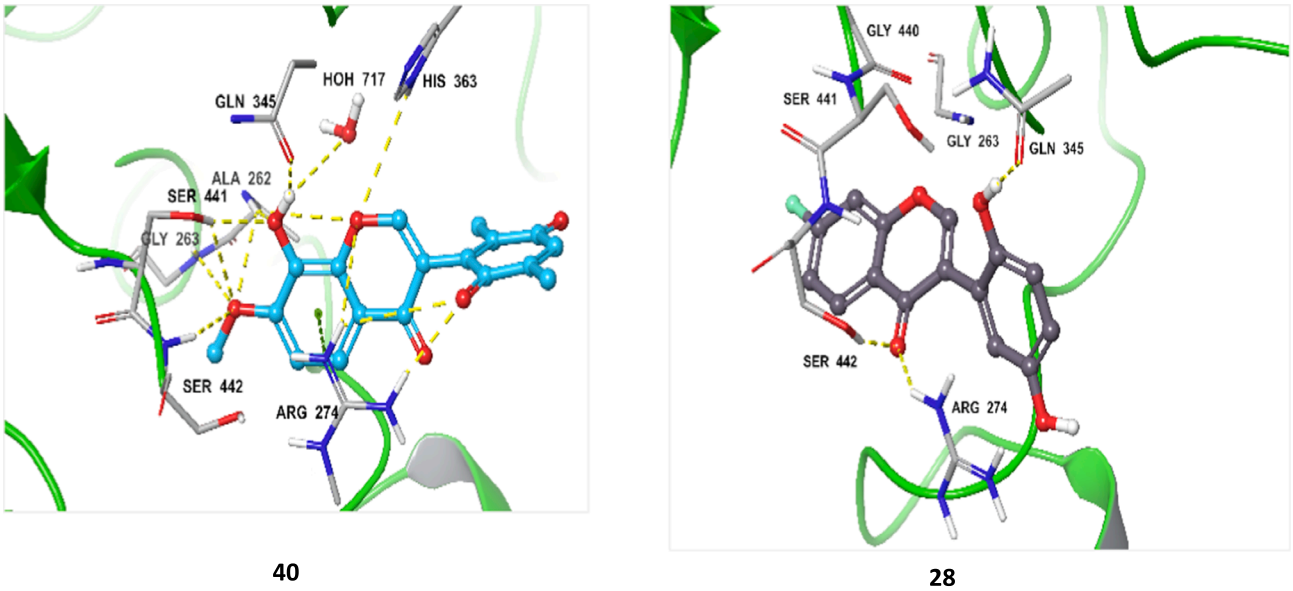

Fig. 6. Predicted binding modes of compounds **40** and **28** at the active site of SIRT1. Protein-ligand interactions are shown as dashed lines; hydrogen bond (yellow), pi-cation (green).

moiety did not improve potency as established by the loss of hydrogen bond interactions, which were seen on complexes bearing a methoxy substituent.

Furthermore, the inferiority of compound **32** antiproliferative effects was replicated in its SIRT1 complex which showed the lowest docking score of −6.083 and binding free energy of −54.43 kcal.mol^{-1}. This was further illustrated by a few hydrogen bond interactions between the target and compound **32** (Fig. 7). The hydroquinone hydroxy groups formed hydrogen bond interaction with Ser441 and Asp272, respectively. Arg274 formed a *pi*-cation interaction with the hydroquinone ring and a hydrogen bond with chromene carbonyl unit.

3. Conclusion

In summary, we have formally identified isoflavone analogues as potent SIRT1 inhibitors. The discovery of the isoflavone-based SIRT1 inhibitors with antiproliferative effects on MDA-MB-231 cancer cells provides new lead compounds which could be utilized in the development of more potent derivatives for TNBC and other cancers. The TNBC is reported to be highly aggressive and metastatic. Therefore, the development of new small molecules that modulate SIRT1 is important for further investigation of the role of SIRT1 in this breast cancer type and other cancers.

4. Experimental

4.1. General procedures and synthesis of benzoylbenzofurans and isoflavones

Previously reported general procedures were followed [23] and benzoylbenzofurans and isoflavone analogues were prepared by the procedures reported by Kunyane *et al* [23].

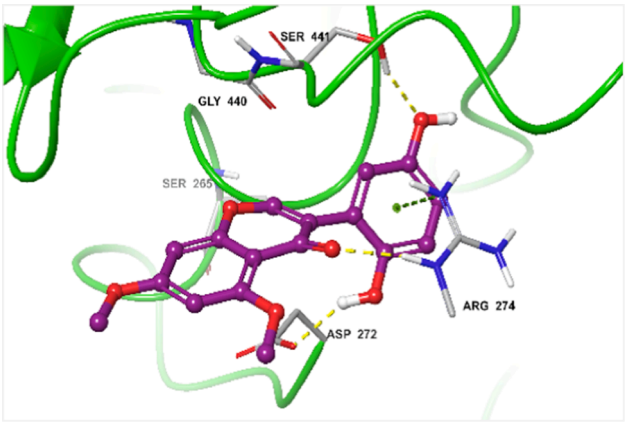

32

Fig. 7. Predicted binding modes of compound **32** at the active site of SIRT1. Protein-ligand interactions are shown as dashed lines; hydrogen bond (yellow), pi-cation (green).

4.1.1. 2-Hydroxy-4,5-methylenedioxyacetophenone (2)

To a stirred solution of sesamol (**1**) (3.0 g, 22 mmol) in acetic anhydride (4.2 mL) under argon atmosphere, boron trifluoride etherate (5.5 mL, 44 mmol) was added dropwise and the reaction mixture was stirred at 80 °C for 8 h. Ice cold water (50 mL) was added and the mixture was extracted with ethyl acetate (3 × 50 mL). The combined organic extracts were washed with brine (50 mL), dried over anhydrous $MgSO_4$, concentrated under reduced pressure, and purified by flash chromatography on silica gel (eluent = hexanes/ ethyl acetate 7:3) to afford product **2** as white crystals (2.48 g, 13.8 mmol, 61%). ^{1}H NMR (400 MHz, DMSO-d_6): δ 2.54 (s, 3H, $COCH_3$); 6.08 (s, 2H, OCH_2O); 6.57 (s, 1H, H-3); 7.39 (s, 1H, H-6); 12.98 (s, 1H, OH-2). ^{13}C NMR (100 MHz, DMSO-d_6): δ 26.9 (CH_3, $COCH_3$); 98.0 (CH, C-3); 102.2 (CH_2, OCH_2O); 108.1 (CH, C-6); 140.3 (C, C-5); 154.2 (C, C-4); 160.9 (C, C-2); 202.9 (C═O). HRMS-ESI *m/z* $[M + H]^+$ 181.0501 (calcd. for $C_9H_9O_4$ 181.0496). IR ν_{max} 3120, 2936, 1718, 1631, 1483, 1429, 1318, 1254, 1179, 1031, 970, 843 cm^{-1}

4.1.2. 2-Methoxy-4,5-methylenedioxyacetophenone (3)

To a stirred mixture of 2-hydroxy-4,5-methylenedioxyacetophenone (**2**) (2.3 g, 12.0 mmol) and K_2CO_3 (3.5 g, 25 mmol) in dry DMF (20 mL) at 100 °C under argon atmosphere was added iodomethane (1.2 mL, 19 mmol). The reaction mixture was stirred at 100 °C for 4 h. After cooling to room temperature, K_2CO_3 was filtered and washed with excess ethyl acetate. The organic layer was washed with water (3 × 50 mL) and then with brine (50 mL), dried over anhydrous $MgSO_4$, filtered, and concentrated *in vacuo*. The crude product was purified by flash chromatography on silica gel (eluent = hexanes/ ethyl acetate 7:3) to afford compound **3** as a white solid (2.16 g, 11.1 mmol, 87%). ^{1}H NMR (400 MHz, $CDCl_3$): δ 2.50 (s, 3H, $COCH_3$); 3.80 (s, 1H, OCH_3-2); 5.91 (s, 2H, OCH_2O); 6.47 (s, 1H, H-3); 7.26 (s, 1H, H-6). ^{13}C NMR (100 MHz, $CDCl_3$): δ 31.9 ($COCH_3$); 56.1 (CH_3, OCH_3-2); 94.1 (CH, C-3); 101.9 (CH_2, OCH_2O); 109.0 (CH, C-6); 120.4 (C, C-1); 141.5 (C, C-5); 152.4 (C, C-4); 157.1 (C, C-2); 197.1 (C═O). HRMS-ESI *m/z* $[M + H]^+$ 195.0663 (calcd. for $C_{10}H_{11}O_4$ 195.0652). IR ν_{max} 1630, 1483, 1421, 1363, 1318, 1254, 1179, 1031, 955 cm^{-1}

4.1.3. 5-Hydroxy-3-(2′-methoxy-4′,5′-methylenedioxybenzoyl)benzo[b] furan (4)

2-Methoxy-4,5-methylenedioxyacetophenone (**3**) (1.0 g, 5.2 mmol) and *N*,*N*-dimethylformamide dimethylacetal (1.73 mL, 13 mmol) were stirred at 100 °C for 12 h under argon atmosphere. After completion, the reaction mixture was concentrated *in vacuo* to give crude enaminone which was used in the next reaction without further purification. *Para*-benzoquinone (0.67 g, 6.2 mmol) and acetic acid (2 mL) were added to a stirred solution of crude enaminone. The reaction mixture was stirred at room temperature for 12 h, quenched with ice cold water, and extracted with ethyl acetate (3 × 50 mL). The combined organic layers were washed with brine and dried under anhydrous $MgSO_4$. The solvent was removed under vacuum and the crude mixture was purified by silica gel column chromatography to afford the benzoylbenzofuran **4** as a light-pink fluffy solid (0.71 g, 2.3 mmol, 44 %). Mp = 239–242 °C. ^{1}H NMR (400 MHz, DMSO-d_6): δ 3.67 (s, 3H, OCH_3-2′); 6.08 (s, 2H, OCH_2O); 6.83 (dd, J = 8.9, 2.5 Hz, 1H, H-6); 6.96 (s, 1H, H-3′); 7.00 (s, 1H, H-6′); 7.42 (d, J = 2.8 Hz, 1H, H-4); 7.47 (d, J = 8.9 Hz, 1H, H-7), 8.35 (s, 1H, H-2); 9.46 (s, 1H, OH-5). ^{13}C NMR (100 MHz, DMSO-d_6): δ 56.5 (CH_3, OCH_3-2′); 95.8 (CH, C-3′); 101.8 (CH_2, OCH_2O); 106.3 (CH, C-4); 108.3 (CH, C-6′); 112.1 (CH, C-7); 114.2 (CH, C-6); 121.5 (C, C-1′); 121.9 (C, C-3); 125.2 (C, C-3a); 140.7 (C, C-5′); 149.1 (C, C-7a); 150.2 (C, C-4′); 153.3 (C, C-2′); 154.7 (C, C-5); 155.3 (CH, C-2); 188.5 (C, C═O). HRMS-ESI *m/z* $[M + H]^+$ 313.0712 (calcd. for $C_{17}H_{13}O_6$ 313.0707).

4.1.4. 2′,5′-Dimethoxy-6,7-methylenedioxyisoflavone (5)

To a stirred solution of **4** (50 mg, 0.16 mmol) in DMF (2 mL) was added trimethylsilyl iodide (1.1 mL, 1.5 mmol) and the reaction mixture was stirred at 85 °C for 36 h. Upon complete consumption of the starting material, the reaction mixture was quenched with ice water (10 mL) and 10% sodium thiosulphate solution (10 mL) and stirred for 1 h at room temperature. Then 10% HCl (10 mL) was added and stirring was continued for a further 1 h. The mixture was extracted with ethyl acetate (3 × 20 mL). The combined organic extracts were washed with brine (50 mL), dried over anhydrous $MgSO_4$, filtered, and concentrated under reduced pressure. To the resulting crude product in DMF (2 mL), K_2CO_3 (44 mg, 0.32 mmol) and iodomethane (0.02 mL, 0.32 mmol) were added. The reaction mixture was stirred at 100 °C for 3 h. After cooling, K_2CO_3 was filtered and washed with excess ethyl acetate. The organic layer was washed with water (3 × 30 mL) and then with 50 mL of brine, dried over anhydrous $MgSO_4$, filtered, and concentrated *in vacuo*. The mixture containing the crude product was purified by flash chromatography on silica gel (eluent = hexanes/ ethyl acetate 6:4) to afford the target product **5** as a yellow solid (18 mg, 0.055 mmol, 34%). Mp = 157–160 °C. ^{1}H NMR (500 MHz, DMSO-d_6): δ 3.66 (s, 3H, OCH_3-2′); 3.72 (s, 3H, OCH_3-5′); 6.23 (s, 2H, OCH_2O); 6.85 (d, J = 3.1 Hz, 1H, H-6′); 6.94 (dd, J = 9.0, 3.1 Hz, 1H, H-4′); 7.01 (d, J = 9.0 Hz, 1H, H-3′); 7.30 (s, 1H, H-8); 7.37 (s, 1H, H-5); 8.26 (s, 1H, H-2). ^{13}C NMR (125 MHz, DMSO-d_6): δ 55.5 (CH_3, OCH_3-5′); 56.1 (CH_3, OCH_3-2′); 98.3 (CH, C-8); 101.3 (CH, C-5); 102.9 (CH_2, OCH_2O); 112.4 (CH, C-3′); 114.0 (CH, C-4′); 117.5 (CH, C-6′); 118.5 (C, C-4a); 121.4 (C, C-3); 121.9 (C, C-1′); 146.1 (C, C-6); 151.6 (C, C-2′); 152.6 (C, C-8a); 152.8 (C, C-7); 153.0 (C, C-5'); 154.2 (CH, C-2); 173.7 (C═O, C-4). HRMS-ESI *m/z* $[M + H]^+$ 327.0876 (calcd. for $C_{18}H_{15}O_6$ 327.0863).

4.2. SIRT1 enzyme assay

The SIRT1 enzyme assay was performed by Reaction Biology Corporation (Malvern, US) using a fluorogenic peptide from p53 residues 379–382 (RHKK(Ac)AMC) as a substrate for SIRT1, which was deacetylated in the presence of NAD^+. For initial screening, the compounds were tested in single dose duplicate mode at a concentration of 100 μM. The most active compounds were then tested in triplicate and 5-dose IC_{50} mode with 3-fold serial dilution starting at 100 μM. The IC_{50} values were calculated using the GraphPad Prism 4 program based on a sigmoidal dose–response equation.

4.3. Cell cytotoxicity assay

MDA-MB-231 cells were cultured in DMEM-F12 (Gibco, Dun Laoghaire, Dublin, Ireland) supplemented with 10% fetal bovine serum (FBS) (Gibco, Dun Laoghaire, Dublin, Ireland), and 1% penicillin and streptomycin (Lonza, Walkersville, MD, USA). Cells were plated at a density of 3000 cells per well due to their fast growth nature. In the IC_{50}

study, MDA-MB-231 cells were plated into flat-bottomed 96-well cell culture plates (Greiner Bio-One GmbH, Frickenhausen, Germany) and incubated for 24 h at 37 °C in 5% CO_2 to allow cell attachment overnight. Thereafter, cells were treated with the compounds at different concentrations for 24 h in triplicate. The average of all the experiments is shown as the cell-viability percentage in comparison with the control, which is the untreated cells and considered as 100% viable. The experiment was terminated by adding MTT (Research Organics Inc, Cleveland, USA), diluted in phosphate-buffered saline (PBS) (pH 7.4) to a final concentration of 5 mg/mL, to each well. The plates were covered with foil, due to light sensitivity, and incubated at 37 °C, 5% CO_2 air and relative humidified atmosphere for 4 h. Following incubation, the MTT solution was removed and the formazan solvent dimethyl sulfoxide (DMSO) (Fisher Chemical Pennsylvania, USA), was added. The plate was covered again with foil and placed on a shaker for 15 min. The MTT assay was used to determine the effect of the different compounds on the cell viability by measurement of the enzymatic reduction of yellow tetrazolium to purple formazan crystals by cellular mitochondria, using PhotoRead Software via Apollo LB 913 (Berthold technologies) UV–vis spectrophotometer at a wavelength of 570 nm. The results from the triplicate experiments were averaged. The statistical analysis was performed using Microsoft Office Excel 2019 (Microsoft Corporation, Washington, USA) and GraphPad Prism Software Version 5.01 for Windows (GraphPad Software, San Diego, USA).

4.4. Molecular docking method

The raw target structure of SIRT1 with (PDB ID: 4I5I) was retrieved from Protein Data Bank and obtained the 3D coordinates from Protein Preparation Wizard [30] and Epik [31] using the default workflow. The low energy conformation structures of the most potent compounds **28 32**, **38**, **39,** and **40** were generated by LigPrep [32].

The prepared ligands were docked in the active site of the target using induced-fit docking (IFD) [33] employing typical standard protocols. The usual protocol parameters included defining the receptor's grid box as the centroid of the cognate ligand of SIRT1 and ligands size of $\leq$ 33 Å with a conformational sampling at a 2.5 kcal mol^{-1} energy window. The initial docking stage with glide constituted generating poses that can be docked on the receptor and followed by Prime refinement to an RMSD of 1.8 Å. Subsequently, structures with an energy of 30 kcal.mol^{-1} were submitted for glide redocking with extra precision to account for fall positives. Thereafter, the best receptor-ligand complex was redocked to improve the final pose.

Parameters such as docking score, glide emodel, IFD score, and glide energy was used as the input structure's scoring functions to compute the ligands binding affinity to the target as free energy bind (ΔG bind) using Prime Molecular Mechanics-Generalized Borne Surface Area (MM-GBSA) protocol [34].

Declaration of Competing Interest

The authors declare that they have no known competing financial interests or personal relationships that could have appeared to influence the work reported in this paper.

Data availability

Data will be made available on request.

Acknowledgements

This work is based on the research supported by the National Research Foundation of South Africa (grant numbers: UID: 113964 and UID: 117853); the University of Pretoria and the South African Nuclear Energy Corporation (Necsa SOC Ltd). We thank Reaction Biology Corporation (RBC) for conducting SIRT1 enzyme assays of the compounds. PS thanks the Centre for High-Performance Computing (CHPC), Cape Town, for the supercomputing facilities.

Appendix A. Supplementary material

Supplementary data to this article can be found online at https://doi.org/10.1016/j.bioorg.2022.106101.

References

[1] A. Kumar, S. Chauhan, How much successful are the medicinal chemists in modulation of SIRT1: A critical review, Eur. J. Med. Chem. 119 (2016) 45–69, https://doi.org/10.1016/j.ejmech.2016.04.063.
[2] A. Chalkiadaki, L. Guarente, The multifaceted functions of sirtuins in cancer, Nat. Rev. Cancer 15 (10) (2015) 608–624, https://doi.org/10.1038/nrc3985.
[3] Y.R. Chung, H. Kim, S.Y. Park, I.A. Park, J.J. Jang, J.Y. Choe, Y.Y. Jung, S.A. Im, H. G. Moon, K.H. Lee, K.J. Suh, T.Y. Kim, D.Y. Noh, W. Han, H.S. Ryu, Distinctive role of SIRT1 expression on tumor invasion and metastasis in breast cancer by molecular subtype, Hum. Pathol. 46 (7) (2015) 1027–1035, https://doi.org/10.1016/j.humpath.2015.03.015.
[4] H. Kim, K.-H. Lee, I.A. Park, Y.R. Chung, S.-A. Im, D.-Y. Noh, W. Han, H.-G. Moon, Y.Y. Jung, H.S. Ryu, Expression of SIRT1 and apoptosis-related proteins is predictive for lymph node metastasis and disease-free survival in luminal A breast cancer, Virchows Arch. 467 (5) (2015) 563–570, https://doi.org/10.1007/s00428-015-1815-7.
[5] S.Y. Chung, Y.Y. Jung, I.A. Park, H. Kim, Y.R. Chung, J.Y. Kim, S.Y. Park, S.-A. Im, K.-H. Lee, H.-G. Moon, D.-Y. Noh, W. Han, C. Lee, T.-Y. Kim, H.S. Ryu, Oncogenic role of SIRT1 associated with tumor invasion, lymph node metastasis, and poor disease-free survival in triple negative breast cancer, Clin. Exp. Metastasis 33 (2) (2016) 179–185, https://doi.org/10.1007/s10585-015-9767-5.
[6] M.-S. Jin, C.L. Hyun, I.A. Park, J.Y. Kim, Y.R. Chung, S.-A. Im, K.-H. Lee, H.-G. Moon, H.S. Ryu, SIRT1 induces tumor invasion by targeting epithelial mesenchymal transition-related pathway and is a prognostic marker in triple negative breast cancer, Tumor Biol. 37 (4) (2016) 4743–4753, https://doi.org/10.1007/s13277-015-4231-3.
[7] S. Sinha, S. Sharma, J. Vora, N. Shrivastava, Emerging role of sirtuins in breast cancer metastasis and multidrug resistance: Implication for novel therapeutic strategies targeting sirtuins, Pharmacol. Res. 158 (2020), 104880, https://doi.org/10.1016/j.phrs.2020.104880.
[8] Y. Liu, G. Lou, J.T. Norton, C. Wang, I. Kandela, S. Tang, N.I. Shank, P. Gupta, M. Huang, M.J. Avram, R. Green, A. Mazar, D. Appella, Z. Chen, S. Huang, 6-Methoxyethylamino-numonafide inhibits hepatocellular carcinoma xenograft growth as a single agent and in combination with sorafenib, FASEB J. 31 (12) (2017) 5453–5465, https://doi.org/10.1096/fj.201700306RR.
[9] M. Schnekenburger, E. Goffin, J.-Y. Lee, J.Y. Jang, A. Mazumder, S. Ji, B. Rogister, N. Bouider, F. Lefranc, W. Miklos, V. Mathieu, P. de Tullio, K.-W. Kim, M. Dicato, W. Berger, B.W. Han, R. Kiss, B. Pirotte, M. Diederich, Discovery and characterization of R/S-N-3-cyanophenyl-n'-(6-tert-butoxycarbonylamino-3,4-dihydro-2,2-dimethyl-2h-1-benzopyran-4-yl)urea, a new histone deacetylase class III inhibitor exerting antiproliferative activity against cancer cell lines, J. Med. Chem. 60 (11) (2017) 4714–4733, https://doi.org/10.1021/acs.jmedchem.7b00533.
[10] A.S. Tikhomirov, A.E. Shchekotikhin, Y.-H. Lee, Y.-A. Chen, C.-A. Yeh, V. V. Tatarskiy, L.G. Dezhenkova, V.A. Glazunova, J. Balzarini, A.A. Shtil, M. N. Preobrazhenskaya, P.J. Chueh, Synthesis and characterization of 4,11-diaminoanthra[2,3-*b*]furan-5,10-diones: Tumor cell apoptosis through tNOX-modulated NAD+/NADH ratio and SIRT1, J. Med. Chem. 58 (24) (2015) 9522–9534, https://doi.org/10.1021/acs.jmedchem.5b00859.
[11] X.-J. Liang, T. Finkel, D.-W. Shen, J.-J. Yin, A. Aszalos, M.M. Gottesman, SIRT1 contributes in part to cisplatin resistance in cancer cells by altering mitochondrial metabolism, Mol. Cancer Res. 6 (9) (2008) 1499, https://doi.org/10.1158/1541-7786.MCR-07-2130.
[12] H.-B. Kim, S.-H. Lee, J.-H. Um, M.-J. Kim, S.-K. Hyun, E.-J. Gong, W.K. Oh, C.-D. Kang, S.-H. Kim, Sensitization of chemo-resistant human chronic myeloid leukemia stem-like cells to Hsp90 inhibitor by SIRT1 inhibition, Int. J. Biol. Sci. 11 (8) (2015) 923–934, https://doi.org/10.7150/ijbs.10896.
[13] M. Delman, S.T. Avci, I. Akcok, T. Kanbur, E. Erdal, A. Cagir, Antiproliferative activity of (R)-4'-methylklavuzon on hepatocellular carcinoma cells and EpCAM+/CD133+ cancer stem cells via SIRT1 and Exportin-1 (CRM1) inhibition, Eur. J. Med. Chem. 180 (2019) 224–237, https://doi.org/10.1016/j.ejmech.2019.07.024.
[14] D. Rotili, D. Tarantino, V. Carafa, C. Paolini, J. Schemies, M. Jung, G. Botta, S. Di Maro, E. Novellino, C. Steinkuhler, R. De Maria, P. Gallinari, L. Altucci, A. Mai, Benzodeazaoxaflavins as sirtuin inhibitors with antiproliferative properties in cancer stem cells, J. Med. Chem. 55 (18) (2012) 8193–8197, https://doi.org/10.1021/jm301115r.
[15] D.J. Newman, G.M. Cragg, Natural products as sources of new drugs over the nearly four decades from 01/1981 to 09/2019, J. Nat. Prod. 83 (3) (2020) 770–803, https://doi.org/10.1021/acs.jnatprod.9b01285.
[16] Q.-X. Yue, X. Liu, D.-A. Guo, Microtubule-binding natural products for cancer therapy, Planta Med. 76 (11) (2010) 1037–1043, https://doi.org/10.1055/s-0030-1250073.

[17] Y. Li, D. Kong, B. Bao, A. Ahmad, F.H. Sarkar, Induction of cancer cell death by isoflavone: The role of multiple signaling pathways, Nutrients 3 (10) (2011) 877–896, https://doi.org/10.3390/nu3100877.
[18] Y. Manevich, L. Reyes, C.D. Britten, D.M. Townsend, K.D. Tew, Redox signaling and bioenergetics influence lung cancer cell line sensitivity to the isoflavone ME-344, J. Pharmacol. Exp. Ther. 358 (2) (2016) 199–208, https://doi.org/10.1124/jpet.115.229344.
[19] D.V. Jeyaraju, R. Hurren, X. Wang, N. MacLean, M. Gronda, A. Shamas-Din, M.D. Minden, A.D. Schimmer, and G. Giaever. A novel isoflavone, ME-344, targets the cytoskeleton in acute myeloid leukemia, Oncotarget 7 (31) (2016) 49777-49785. https://doi.org/10.18632/oncotarget.10446.
[20] M.W. Saif, A. Heaton, K. Lilischkis, J. Garner, D.M. Brown, Pharmacology and toxicology of the novel investigational agent cantrixil (TRX-E-002-1), Cancer Chemother. Pharmacol. 79 (2) (2017) 303–314, https://doi.org/10.1007/s00280-016-3224-2.
[21] A.B. Alvero, A. Heaton, E. Lima, M. Pitruzzello, N. Sumi, Y. Yang-Hartwich, C. Cardenas, S. Steinmacher, D.-A. Silasi, D. Brown, G. Mor, TRX-E-002-1 induces c-Jun-dependent apoptosis in ovarian cancer stem cells and prevents recurrence in vivo, Mol. Cancer Ther. 15 (6) (2016) 1279–1290, https://doi.org/10.1158/1535-7163.MCT-16-0005.
[22] A.I. Green, G.M. Burslem, Focused libraries for epigenetic drug discovery: The importance of isosteres, J. Med. Chem. 64 (11) (2021) 7231–7240, https://doi.org/10.1021/acs.jmedchem.1c00592.
[23] P. Kunyane, M.S. Sonopo, M.A. Selepe, Synthesis of isoflavones by tandem demethylation and ring-opening/cyclization of methoxybenzoylbenzofurans, J. Nat. Prod. 82 (11) (2019) 3074–3082, https://doi.org/10.1021/acs.jnatprod.9b00681.
[24] G. Kremmidiotis, A.F. Leske, T.C. Lavranos, D. Beaumont, J. Gasic, A. Hall, M. O'Callaghan, C.A. Matthews, B. Flynn, BNC105: A novel tubulin polymerization inhibitor that selectively disrupts tumor vasculature and displays single-agent antitumor efficacy, Mol. Cancer Ther. 9 (6) (2010) 1562–1573, https://doi.org/10.1158/1535-7163.MCT-09-0815.
[25] B.L. Flynn, G.S. Gill, D.W. Grobelny, J.H. Chaplin, D. Paul, A.F. Leske, T. C. Lavranos, D.K. Chalmers, S.A. Charman, E. Kostewicz, D.M. Shackleford, J. Morizzi, E. Hamel, M.K. Jung, G. Kremmidiotis, Discovery of 7-hydroxy-6-methoxy-2-methyl-3-(3,4,5-trimethoxybenzoyl)benzo[*b*]furan (BNC105), a tubulin polymerization inhibitor with potent antiproliferative and tumor vascular disrupting properties, J. Med. Chem. 54 (17) (2011) 6014–6027, https://doi.org/10.1021/jm200454y.
[26] T. Wang, C. Wu, C. Wang, G. Zhang, K.E. Arnst, Y. Yao, Z. Zhang, Y. Wang, D. Pu, W. Li, Unraveling the molecular mechanism of BNC105, a phase II clinical trial vascular disrupting agent, provides insights into drug design, Biochem. Biophys. Res. Commun. 525 (1) (2020) 148–154, https://doi.org/10.1016/j.bbrc.2019.12.083.
[27] H. Khanam, Bioactive benzofuran derivatives: A review, Eur. J. Med. Chem. 97 (2015) 483–504, https://doi.org/10.1016/j.ejmech.2014.11.039.
[28] J.T. Ndongo, M.E. Issa, A.N. Messi, J.N. Mbing, M. Cuendet, D.E. Pegnyemb, C. G. Bochet, Cytotoxic flavonoids and other constituents from the stem bark of *ochna schweinfurthiana*, Nat. Prod. Res. 29 (17) (2015) 1684–1687, https://doi.org/10.1080/14786419.2014.991321.
[29] C.A. Stein, Suramin: A novel antineoplastic agent with multiple potential mechanisms of action1, Cancer Res. 53 (10) (1993) 2239–2248.
[30] **Schrödinger Release 2021-2** Protein Preparation Wizard; Epik, Schrödinger, LLC, New York, NY, 2021; Impact, Schrödinger, LLC, New York, NY; Prime, Schrödinger, LLC, New York, NY, 2021.
[31] **Schrödinger Release 2021-2**: Epik, Schrödinger, LLC, New York, NY, 2021.
[32] **Schrödinger Release 2021-2**: LigPrep, Schrödinger, LLC, New York, NY, 2021.
[33] **Schrödinger Release 2021-2**: Induced Fit Docking protocol; Glide, Schrödinger, LLC, New York, NY, 2021; Prime, Schrödinger, LLC, New York, NY, 2021.
[34] **Schrödinger Release 2021-2**: Prime-MMGBSA, Schrödinger, LLC, New York, NY, 2021.